ACS NANO

www.acsnano.org

ARTICLE

Metal–Organic Framework-Based Biosensor for Detecting Hydrogen Peroxide in Plants through Color-to-Thermal Signal Conversion

Yong Yan,[§] Min Ni,[§] Fan Wang,[§] Yue Yu, Xin Gong, Yue Huang, Wei Tao, Chao Li,* and Feng Wang*

Cite This: *ACS Nano* 2022, 16, 15175–15187

Read Online

ACCESS | Metrics & More | Article Recommendations | Supporting Information

ABSTRACT: Plant biotic or abiotic stresses, such as pathogens, mechanical damage, or high temperature, can increase intracellular H_2O_2 concentration, damaging proteins, lipids, and DNA. Most current H_2O_2 detection methods require the separation or grinding of plant samples, inducing plant stresses, and the process is complicated and time-consuming. This paper constructed a metal–organic framework (MOF)-based biosensor for real-time, remote, and *in situ* detection of exogenous/endogenous H_2O_2 in plant organs through color-to-thermal signal conversion. By simply spraying horseradish peroxidase, 2,2′-azino-bis(3-ethylbenzothiazoline-6-sulfonic acid) (ABTS), and the precursor of zeolite imidazolate frameworks-8 (ZIF-8), ZIF-8 biosensors were formed *in situ* on a plant root, petiole, or leaf. This biosensor could report sub-micromolar H_2O_2 in plants since the oxidation products, $ABTS^{\bullet+}$, emitted heat when they absorbed energy from near-infrared (NIR) light. Due to the plant's low absorption in the NIR region, the ZIF-8 biosensor allowed for remote thermal sensing of H_2O_2 transport or biotic/abiotic stresses in plants with a high signal-to-noise ratio combining NIR laser and thermometer. Our biosensor can be used for the future development of plant sensors for monitoring plant signaling pathways and metabolism that are nondestructive, minimally invasive, and capable of real-time, *in situ* analysis.

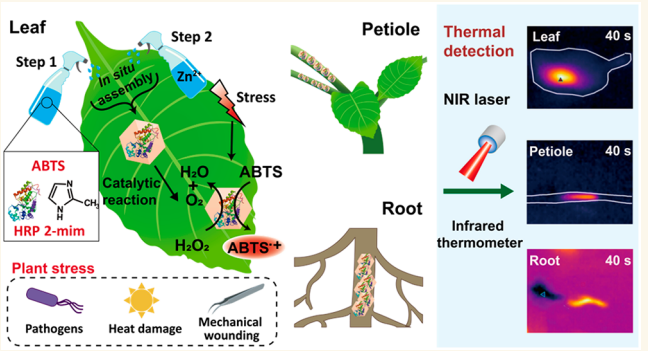

KEYWORDS: *biosensor, hydrogen peroxide, metal–organic framework, plant stress, thermal signal*

INTRODUCTION

Environmental pollution, global warming, and climate change exacerbate the impact of biotic and abiotic stresses on plant growth, development, and yield.[1−3] Therefore, accurate monitoring and assessing plant physiological status are critical for soil, water, nutrients, pesticide conservation, and crop yield increment.[4−8] Reactive oxygen species (ROS) are a class of essential signaling molecules involved in mediating cell-to-cell communication to activate plant defense mechanisms.[9,10] Hydrogen peroxide (H_2O_2) is the critical ROS that mediates rapid system signal transduction in plants and is regarded as an acute stress indicator.[11,12] Environmental stress conditions, such as heat, mechanical wounding, salinity, cold, or pathogen infection, can produce a large amount of H_2O_2, which activates regulatory mechanisms and biotic/abiotic stress response in plants.[13] As stated above, H_2O_2 as an essential signal molecule may play a crucial role under various biotic/abiotic stress conditions and is closely associated with plant health. Monitoring the level of H_2O_2 in plant organs (*i.e.*, leaves, roots, petioles) can give us a sense of how plants respond to biotic/abiotic stresses, which is highly valuable for agriculture biosensing.

Current techniques for detecting H_2O_2 signals are limited to fluorescent dyes, histochemical reagents, electrochemical sensing, and nanosensors such as carbon nanotubes.[13−17] However, due to chlorophyll autofluorescence interference, conventional fluorescent methods are difficult to apply directly to plant organs.[18] Histochemical staining needs a cumbersome and long-time extraction and staining operation, which can not be used to monitor H_2O_2 in real-time and *in situ*. Electrochemical detection provides an attractive means to monitor H_2O_2 while requiring modification of the indium tin oxide working electrode.[17] As a result, nondestructive analysis of the

Received: July 1, 2022
Accepted: September 7, 2022
Published: September 8, 2022

Scheme 1. Cartoon Illustration of ZIF-8-Based Plant H_2O_2 Biosensor[a]

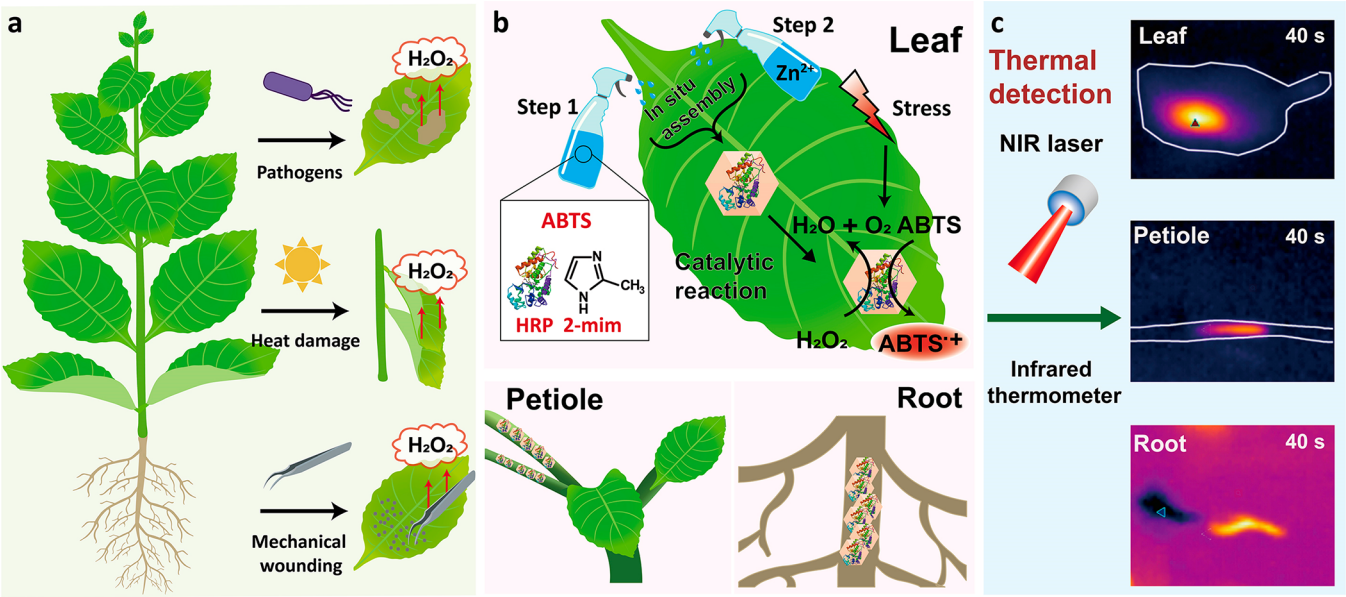

[a](a) *Nb* under different stresses, such as pathogens, heat damage, mechanical wounding, and generating endogenous H_2O_2. (b) HPR and ABTS are *in situ* encapsulated during ZIF-8 formation on plant organ surfaces (*i.e.*, leaves, roots, petioles) via a spray method. Step 1: HPR, ABTS, and 2-methylimidazole (2-mim) are mixed and sprayed onto plant organ surfaces. Step 2: Zn^{2+} solution is further sprayed at the same site. Exogenous/endogenous H_2O_2 acts as a signal molecule and oxidizes ABTS to its free radical, $ABTS^{\bullet+}$. (c) $ABTS^{\bullet+}$ generates thermal signals under a NIR laser captured by a thermometer.

level of H_2O_2 and its transportation in plants remains a formidable task. Nanotechnology and nanobionics emerged as essential tools for monitoring plant signaling pathways and metabolism using a nondestructive and minimally invasive manner.[19−21] Emerging wearable sensors were also designed for plant health monitoring by profiling various biomarkers and transducing signals to electric readout for plant physiology and pathological analysis.[22,23] Lew *et al.* developed a near-infrared (NIR) fluorescent biosensor based on H_2O_2-selective DNA-wrapped single-walled carbon nanotubes (SWCNT), which could nondestructively, real-time monitor the H_2O_2 signal transduction pathway induced by wounds in model plants and nonmodel plants.[13] Besides, the NIR fluorescence of SWCNT avoided the autofluorescence window of plant organs, allowing for the detection of H_2O_2 with a high signal-to-noise (S/N) ratio. Wu *et al.* noncovalent modified chiral SWCNT with porphyrins and their aptamers for monitoring the level of H_2O_2 with the onset of plant stress.[24] Compared to traditional *in vitro* methods, H_2O_2-responsive SWCNT offers a convenient, straightforward, and dynamic means for spatiotemporal monitoring analytes in plant organs, representing the next-generation plant sensors. Despite these advantages, SWCNT-based plant biosensors have some inevitable questions, which significantly impede the application of biosensors in plants. First, these biosensors are infused into plant organs using a syringe, and the thick wax shells on plant organ surfaces make it difficult to be infused with an external solution. Moreover, the leaf infiltration method is challenging to be implemented on other organs (*e.g.*, root, petiole, and stem) due to their small size. Second, SWCNT-based plant biosensors are signal-off fluorescent devices, and the sensitivity is directly associated with biosensors' quality and environmental conditions. Therefore, exploiting more biosensors for plant analysis is in its infancy. It remains challenging to develop straightforward, real-time, remote, and sensitive biosensors for *in situ* analysis of H_2O_2 in plants.

Metal−organic frameworks (MOFs) are porous nanomaterials that consist of metal ions and organic linkers.[25,26] MOFs can encapsulate various biomolecules, such as nucleic acids, proteins, polysaccharides, and even whole cells.[27−30] Once encapsulated in MOFs, there is a significant enhancement in biomolecule chemical stability and biological activities under harsh conditions.[31,32] Various biomolecule/MOF hybrids have been developed with their applications in catalysis,[33] cancer therapy,[34−37] biosensing,[38,39] and detoxification.[40] Moreover, MOFs can be assembled on both hydrophilic and hydrophobic surfaces owing to intermolecular interactions provided by metal nodes and organic linkers.[41] Liang's group reported two types of MOFs inside living plants. One of the luminescent lanthanide MOFs could be utilized for small molecule and environmental pollutant sensing.[42,43] Li *et al.* developed a triboelectric nanogenerator based on surface-attached MOF coating on plant leaves and explored this triboelectric nanogenerator as a plant photosynthesis sensor.[44] We anticipate that MOFs can encapsulate recognition and signal elements based on these merits, acting as remote sensors to report plant status.

Herein, we developed a straightforward and sensitive method for assembling MOF-based biosensors on plant organs, using temperature as the signal readout to detect exogenous/endogenous H_2O_2. As illustrated in Scheme 1, horseradish peroxidase (HPR) and 2,2′-azino-bis (3-ethylbenzothiazoline-6-sulfonic acid) (ABTS) were *in situ* encapsulated during zeolite imidazolate frameworks-8 (ZIF-8) formation on different plant organ surfaces, including leaves, roots, and petioles, *via* a spray method. This ZIF-8 biosensor has several merits for analyzing H_2O_2 in plants: (1) The ZIF-8 biosensor preparation on plant organ surfaces is straightforward, rapid, and convenient under mild conditions (*i.e.*, an

https://doi.org/10.1021/acsnano.2c06481
ACS Nano 2022, 16, 15175−15187

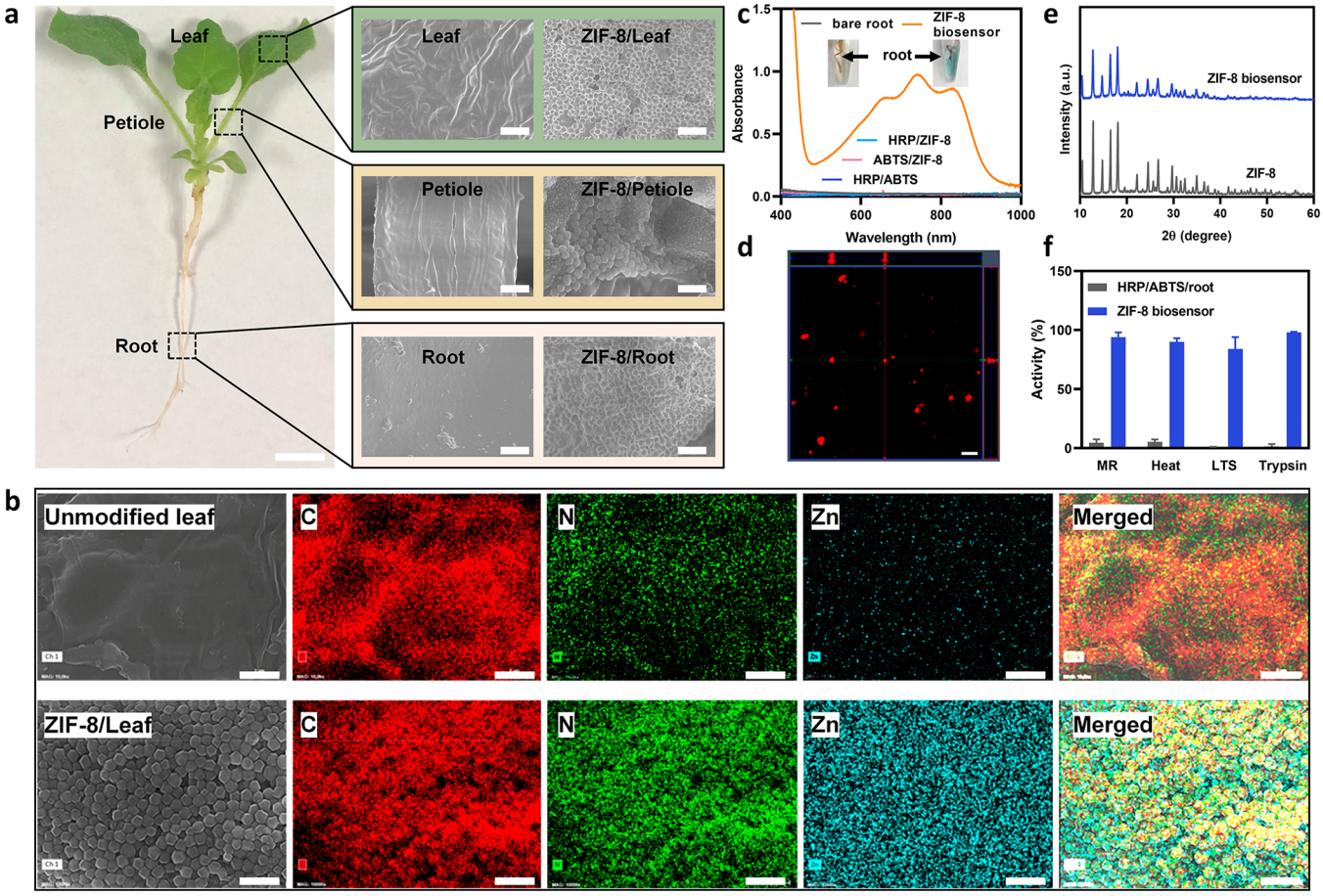

Figure 1. (a) Typical *Nb* and SEM images showing unmodified or modified plant surfaces with numerous polyhedral structures around 550 nm on *Nb* leaf, root, and petiole surfaces. Scale bar: 2 cm for *Nb* plant and 2 μm for SEM images. (b) Elemental composition analysis of the unmodified and ZIF-8-coated *Nb* leaf. Scale bar: 2 μm. (c) UV/vis spectroscopy of bare root, HRP/ZIF-8-, ABTS/ZIF-8-, ABTS/HRP-, and ZIF-8-biosensor-coated roots in H_2O_2 (50 μM) solution. Inlet: images with bare root or ZIF-8 biosensor-coated root in H_2O_2 (50 μM) solution. (d) Microscopy Z-stack image showing HRP encapsulated in ZIF-8. Scale bar: 5 μm. (e) XRD patterns of pure ZIF-8 and ZIF-8 biosensors. (f) Stability of HRP and ZIF-8 biosensor coated on *Nb* roots under different harsh treatments, including multirinsing steps (MR), heat at 60 °C for 15 min, long-term storage for 7 days (LTS), and trypsin digestion.

aqueous solution). Besides, the ZIF-8 biosensor can be robustly assembled on different plant organ surfaces, avoiding cumbersome and position-limited infusion operations with SWCNT-based biosensors. (2) HRP as the critical recognition element ensures high sensitivity and specificity to H_2O_2 since it is one of the most efficient natural enzymes and highly specific to H_2O_2.[45,46] Moreover, HPR itself is purified from the tuberous roots of the horseradish plant. Therefore, this enzyme can adapt to the plant environment and fully execute its function. Unlike traditional signal-off sensors,[47] our signal-on biosensor reduces false-positive results from the complex physiological environment, further improving the S/N ratio. (3) The chemical stability and enzyme activity of the HRP-ABTS system can be well-persevered once encapsulated into the ZIF-8 exoskeleton. (4) Plant organs have strong autofluorescence while their NIR absorption is relatively low. Owing to the bright green plant leaf color, direct H_2O_2 detection through HRP-catalyzed H_2O_2 decomposition and blue-green colored ABTS oxidative product was not easy. Due to the increased NIR absorbance of the ABTS oxidative product, our ZIF-8-based biosensor takes the simple color-to-thermal (temperature) signal readout conversion. This biosensor can also realize the nondestructive and *in situ* H_2O_2 detection in plant organs by combining NIR laser and thermometer, which helps understand the transport of H_2O_2 in plant organs and how plants counter biotic and abiotic stresses.[48]

RESULTS AND DISCUSSION

Formation of Biosensors on Various Plant Organ Surfaces. *Nicotiana benthamiana* (*Nb*) was a model plant for studying plant biotic and abiotic stresses.[49] The ZIF-8-based biosensor formation on different *Nb* organ surfaces is shown in Figure S1. Unlike pure ZIF-8 or HRP/ZIF-8 composite, rapid construction of the ZIF-8 biosensor, *i.e.*, ABTS/HRP/ZIF-8 composite, was detected with a 5 min reaction time. After repeated washing, white patches on *Nb* organs existed only with the ZIF-8 biosensor, demonstrating its higher adsorbing capacity on *Nb* organ surfaces. It was reasonable that *Nb* organs without ZIF-8 modification did not have any white patches (Figure S1). Scanning electron microscopy (SEM) analysis revealed that numerous polyhedral structured particles with a uniform size of ~550 nm were on *Nb* leaf, petiole, and root surfaces after ZIF-8 biosensor modification (Figure 1a). According to the SEM coupled with an energy dispersive spectrometer (EDS), there presented abundant elements, such as zinc and nitrogen, on the modified *Nb* leaf, suggesting the

https://doi.org/10.1021/acsnano.2c06481
ACS Nano 2022, 16, 15175−15187

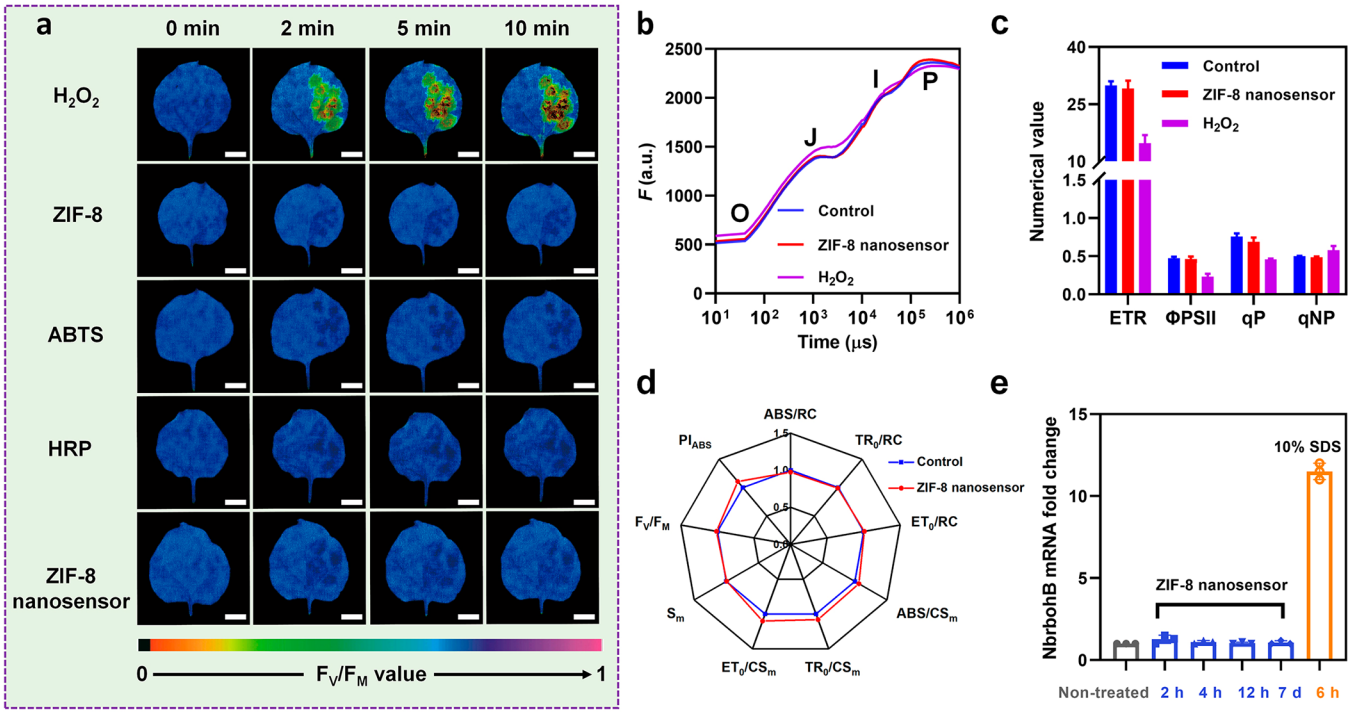

Figure 2. Photosynthesis and gene-level biocompatibility of the ZIF-8 biosensor. (a) Chlorophyll fluorescence images of *Nb* leaves treated with H_2O_2, ABTS, ZIF-8, HRP, and ZIF-8 biosensor. [H_2O_2] = 1 mM, [HRP] = 15 μg mL^{-1}, [ABTS] = 2 mg mL^{-1}. Plants with F_V/F_M value of around 0.7 are considered free of stress. Scale bar: 1 cm. (b) Transient chlorophyll fluorescence induction curves. (c) Chlorophyll fluorescence parameters of *Nb* leaves spraying the ZIF-8 biosensor. H_2O_2 (50 μL, 1 mM) solution was used as a positive toxicity control. (d) Radar plot of chlorophyll fluorescence parameters of *Nb* leaves before and after spraying the ZIF-8 biosensor under dark adaptation. (e) qPCR analysis of *NbrbohB* stress gene expression. 10% SDS solution was used as a positive control. No long-term toxicity for ZIF-8 biosensor-modified leaves.

successful coating of the ZIF-8 biosensor on the *Nb* leaf (Figure 1b). Due to the electrostatic and coordination interaction, the element zinc was found all over the *Nb* leaf. Moreover, the organic linker, *i.e.*, 2-mim, provided complementary binding forces, such as van der Waals force, hydrophobic interaction, and hydrogen bonding for the attachment of ZIF-8 biosensors on plant organ surfaces.[50] We also provided more information, *i.e.*, SEM image and EDS results, on ZIF-8 in an aqueous solution (Figure S2). No changes in the ZIF-8 morphology were with ZIF-8 in an aqueous solution or sprayed onto *Nb* leaves.

To confirm that HRP and ABTS were encapsulated into the ZIF-8 exoskeleton, after multiple washing steps, we immersed the ZIF-8-coated root in a 50 μM H_2O_2 solution. Untreated root did not induce any color change. The color of the H_2O_2 solution remained unchanged for the *Nb* root coating ZIF-8 encapsulated with HRP or ABTS (HRP/ZIF-8 or ABTS/ZIF-8). In contrast, the H_2O_2 solution turned green within 1 min after introducing ZIF-8 biosensors. Ultraviolet−visible (UV−vis) spectroscopy confirmed that H_2O_2 in solution could oxidize ZIF-8 biosensors on *Nb*, generating $ABTS^{\bullet+}$ with characteristic optical absorption ranging from 400 to 900 nm. On top of that, no noticeable color change could be seen with bare roots, ABTS/HRP-, HRP/ZIF-8-, and ABTS/ZIF-8-coated roots after thoroughly washing (Figure 1c). Therefore, we came to the following conclusions: first, neither HRP nor ABTS adsorbed onto plant organs, emphasizing the importance of ZIF-8 encapsulation; second, HRP and ABTS, should be encapsulated inside the ZIF-8 exoskeleton where H_2O_2 in solution could oxidize ABTS catalyzed by HRP. The distribution of fluorescence signals along the *z*-axis obtained *via* confocal laser scanning microscopy (CLSM) demonstrated that HPR and ABTS remained trapped in the ZIF-8 biosensor after repeated washing using rhodamine-labeled HRP (Rh-HRP) (Figure 1d and Figure S3). Therefore, HRP was successfully encapsulated in the interior of the ZIF-8 exoskeleton. X-ray diffraction (XRD) experiments were performed to determine the crystal structure. A similar diffraction pattern was shown in the ZIF-8 biosensor, revealing that HRP and ABTS encapsulation did not affect the crystallographic structure of ZIF-8 (Figure 1e). UV/vis and bicinchoninic acid (BCA) assay were used to determine the encapsulation efficiency of HRP and ABTS, which were 15% and 98.7%, respectively (Figure S4).

Next, we evaluated the stability of the ZIF-8 biosensor on *Nb* root surfaces. The HRP/ABTS mixture added to the H_2O_2 solution was used as the positive control. ZIF-8 biosensors could respond to H_2O_2 after several harsh treatments, including multirinsing steps (MR), heating at 60 °C for 15 min, long-term storage for 7 days (LTS), and trypsin digestion. In contrast, the *Nb* root sprayed with HRP/ABTS failed to generate any colorimetric signal following the same process, which was reasonable since unprotected HRP could lose its catalytic activity under harsh environmental conditions (Figure 1f).

We further evaluated the sensing performance of the ZIF-8 biosensor for H_2O_2 detection *in vitro*. UV−vis absorption spectrum values in the presence of different concentrations of H_2O_2 indicated that the ZIF-8 biosensor was a good colorimetric sensing platform to detect H_2O_2 (Figure S5a).

https://doi.org/10.1021/acsnano.2c06481
ACS Nano 2022, 16, 15175−15187

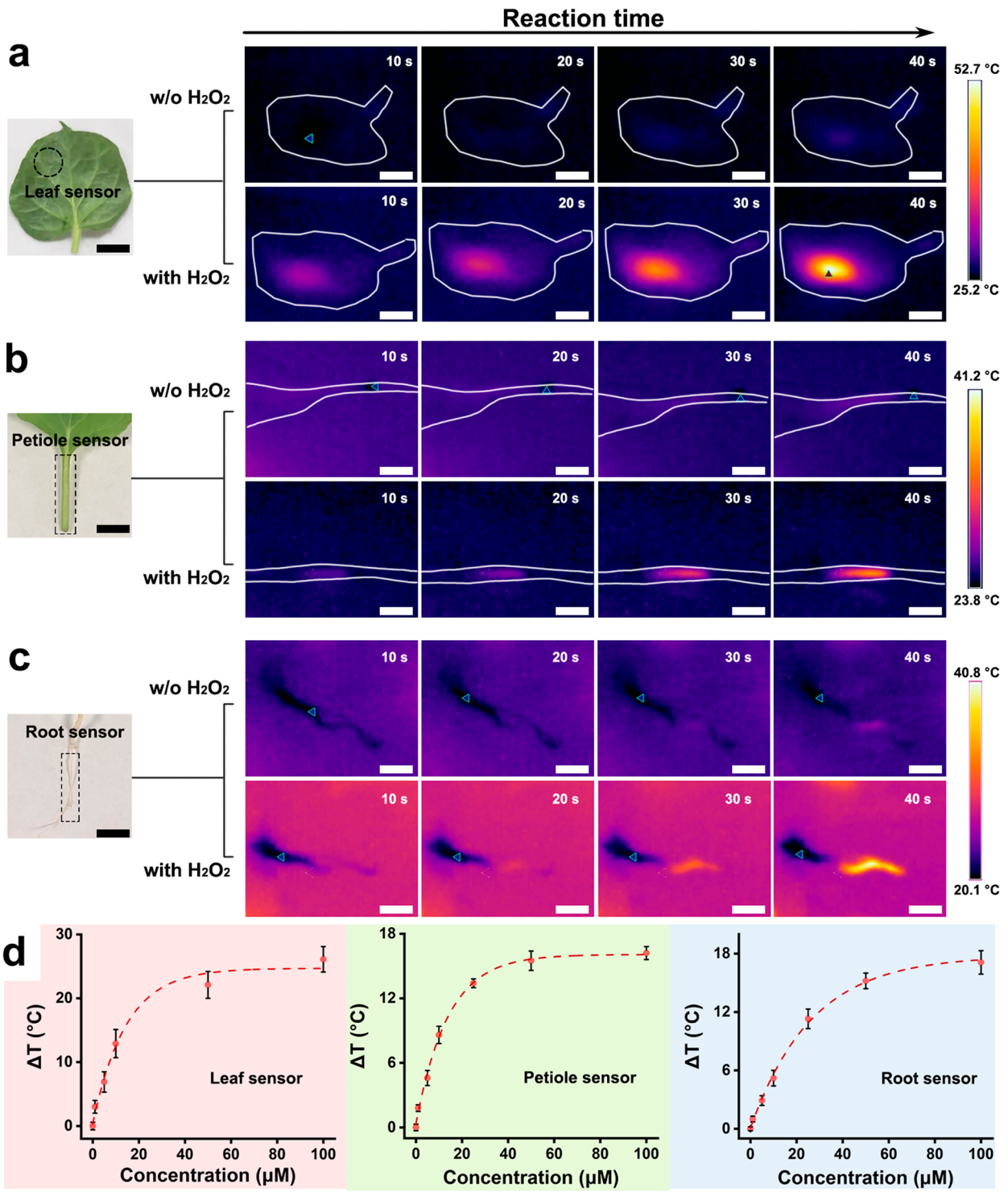

Figure 3. ***In situ*** **thermal imaging of the fabricated biosensors on** ***Nb*****'s (a) leaf, (b) petiole, and (c) root under NIR light irradiation (808 nm, 2 W cm^{-2}) with or without adding 50 μM H_2O_2. The white lines outlined** ***Nb*** **organs. Scale bar: 1 cm. (d) Calibration curves of leaf, petiole, and root sensors for H_2O_2 detection using the thermal signal.**

The parameters for H_2O_2 detection were optimized. As shown in Figure S6, H_2O_2 concentration was fixed at 100 μM. Notably, the pH of 100 μM H_2O_2 is 5.8, which is quite similar to Milli-Q water (weak acidity due to the dissolution of carbon dioxide). Therefore, in this pH condition, the ZIF-8 biosensor should be stable in the experiment's time frame (Figure S7). The optimized experimental conditions for detection H_2O_2 were set as follows: ABTS 2 mg mL^{-1}; HRP 15 μg mL^{-1}; reaction time 5 min. Under the optimal condition, the limit of detection (LOD, 3σ/k) was 120 nM (Figures S5b and S6). This sensitivity was superior to pure HRP analysis, suggesting that HRP and ABTS coencapsulated into ZIF-8 offered a distinct microenvironment for catalysis reaction (Figure S8). Furthermore, photothermal images and the temperature of ZIF-8 biosensor solution with or without H_2O_2 were recorded under the 808 nm laser irradiation. With 100 μM H_2O_2, the

https://doi.org/10.1021/acsnano.2c06481
ACS Nano 2022, 16, 15175−15187

temperature of the solution increased from 23.5 to 72.5 °C within 30 s, whereas minor changes were without H_2O_2 (Figure S5c). Under the optimized NIR conditions (808 nm, 2 W cm^{-2}), an H_2O_2 concentration-dependent thermal signal increase was presented with a LOD estimated to be 510 nM (Figures S5d and S9). However, this LOD is obtained in an H_2O_2 solution. The endogenous H_2O_2 concentration in plant organs typically ranges from 1 to 100 μM. The LOD of our ZIF-8 biosensor in plant tissue should be further investigated in the following sections.

Biocompatibility of ZIF-8 Biosensors on Plants. When the ZIF-8 biosensor is deployed for plant applications, we need first to ensure the biosensor's biocompatibility. Physiological changes of plants were affected by biotic and abiotic stresses. F_V/F_M, the ratio of variable to maximum fluorescence after dark adaptation, is a crucial indicator of plant photosynthetic performance, and lower values can indicate plant biotic and abiotic stresses.[51,52] According to F_V/F_M values in Figure 2a, no stressed leaves were with the ZIF-8 biosensor and its components, *i.e.*, ZIF-8, ABTS, and HRP, indicating that the ZIF-8 biosensor and its components had no toxicity for *Nb*. In contrast, a pronounced F_V/F_M decrease could be detected by applying exogenous H_2O_2, suggesting that *Nb* leaf was under significant stress. Time-resolved chlorophyll fluorescence induction kinetic curves were measured to evaluate the electron transfer chain between PSII and photosystem I (PSI).[53,54] The OJIP transient curve is defined by O, J, I, and P steps and a stress indicator to characterize the effect of biotic and abiotic stresses.[55] ZIF-8 biosensors had a standard three-step OJIP transient with an increase in total fluorescence from the base to the top, the same as the untreated plant leaves (Figure 2b). However, the H_2O_2-treated leaf had a higher fluorescence intensity at the J step and I step, resulting in a dramatically changed OJIP curve shape. Similar to the untreated group, the electron transfer rates (ETRs), actual photochemical efficiency of PSII (ϕPSII), photochemical quenching coefficient (qP), and non-qP (qNP) of ZIF-8 biosensor-treated *Nb* leaf were also performed with no significant changes (Figure 2c). H_2O_2, as a positive stress factor, severely disrupted the chloroplast photosynthetic electron transfer process. The photosynthetic activity of *Nb* was further studied by analyzing the measured chlorophyll fluorescence signals.[56,57] F_V/F_M and other chlorophyll-related test parameters did not change much after coating the ZIF-8 biosensor on the *Nb* leaf, indicating that light energy captured from sunlight and transferred in the photosynthetic electron transport chain was not affected (Figure 2d, Table S1). Respiratory burst oxidase homologues B (*RbohsB*) and *RbohsB* gene expression play a vital role in plant growth, development, and various biotic and abiotic stress responses.[49] Quantitative polymerase chain reaction (qPCR) results showed no *RbohB* gene up-regulation with the ZIF-8 biosensor-treated *Nb* (*Nb* gene *NbrbohB*). 10% SDS solution was further used as a positive toxicity control that up-regulated the *NbrbohB* gene by 10-fold 6 h after spraying (Figure 2e). Overall, photosynthesis and gene-level results suggested that the ZIF-8 biosensor and its components were highly biocompatible with plants.

Thermal Analysis of Exogenous H_2O_2 on Different Plant Organs. Due to the excellent biocompatibility of the ZIF-8 biosensor, we used ZIF-8 biosensors on the *Nb*'s leaf, root, and petiole for H_2O_2 detection. A drop of H_2O_2 solution was added to assembled sites. Although HRP-catalyzed H_2O_2 decomposition and ABTS oxidation in ZIF-8 biosensors could generate blue-green colored radical cation $ABTS^{\bullet+}$, no apparent difference could be seen with H_2O_2 treatment owing to the bright green *Nb* leaf color (Figure S10). This result proved that H_2O_2 in *Nb* leaf could not be reported using colorimetric analysis. Considering the increased NIR absorbance of $ABTS^{\bullet+}$, deploying thermal NIR imaging with our ZIF-8 biosensor was an efficient method for detecting H_2O_2 in plants.[58] Thus, we applied an inexpensive and easy-to-operate NIR thermometer to monitor the temperature change of plant organs under NIR light irradiation (808 nm, 2 W cm^{-2}, 40 s). Using our biosensors with 50 μM H_2O_2, the temperature of leaf, petiole, and root rapidly increased from room temperature to 51.3, 40.2, and 38.8 °C, respectively (Figure 3a–c and Figure S11). Note that irradiated sites without adding H_2O_2 had negligible changes since the elevated temperature was due to H_2O_2 addition. The assembly of pure ZIF-8, ABTS/ZIF-8, or HRP/ZIF-8 on *Nb* leaves was also investigated, and no thermal signals were detected with these treatments, even in a high concentration of H_2O_2 (100 μM) (Figure S12). Therefore, such a ZIF-8 biosensor is indispensable for H_2O_2 detection with high sensitivity. Besides, plant health is reasonably related to environmental temperature. The susceptibility to high temperature in plants depends on species and genotypes. Therefore, once applying this biosensor, the temperature increment should be controlled within a reasonable range. *In situ* thermal imaging of the fabricated biosensors on *Nb*'s leaf, petiole, and root under NIR light irradiation (808 nm, 2 W cm^{-2}) at 1 μM H_2O_2 was also provided in Figure S13. Only the leaf biosensor has 1 °C temperature increase compared to the pure ZIF-8 group. Our ZIF-8 biosensor on *Nb* leaf surfaces could detect H_2O_2 through color-to-thermal signal conversion, and a stable temperature increase (ΔT = 25 °C) was within the time frame of the test (8 days) in Figure S14. It was worth noting that ZIF-8 biosensor preparation on *Nb* leaf surfaces was *via* a spray method. By spraying reactants on plant leaf and repeated washing (number of spraying up to five), the sensing performance depending on the thickness of the ZIF-8 biosensor was provided (Figure S15). One time of spraying showed homogeneous few layers of ZIF-8 particles on the *Nb* leaf surface. However, five times of spraying showed a large amount of ZIF-8 aggregates on *Nb* leaf surface with relatively small particle size. At a lower H_2O_2 (10 μM) concentration, one to five times of spraying had a similar sensing performance (ΔT = 6.5–8.6 °C). At a higher H_2O_2 (50 and 100 μM) concentration, four times of spraying had a 20% increase in temperature sensitivity and five times of spraying was about the same as four times of spraying. Considering the convenience of the experimental operation, ZIF-8 biosensor preparation on *Nb* surfaces was *via* the spray method for only once.

The sensing performance of the ZIF-8 biosensor for H_2O_2 detection was investigated. As shown in Figure 3d, the thermal signal of plant organs increased with increased H_2O_2 concentration. The LODs of leaf, petiole, and root sensors were determined to be 600, 800, and 900 nM, respectively. A sensor's specificity was further evaluated with various stress-related plant metabolites.[59] As plants' main photosynthetic products and nutrients, glucose (Glu) and sucrose (Suc) play a critical role in plant growth, development, stress, and metabolism. In most cases, Glu and Suc act as nutrient signals to regulate plant growth and development.[60] Calcium ions (Ca^{2+}), the most important second messenger in plant cells, are involved in the transduction of many stress signals in

https://doi.org/10.1021/acsnano.2c06481
ACS Nano 2022, 16, 15175–15187

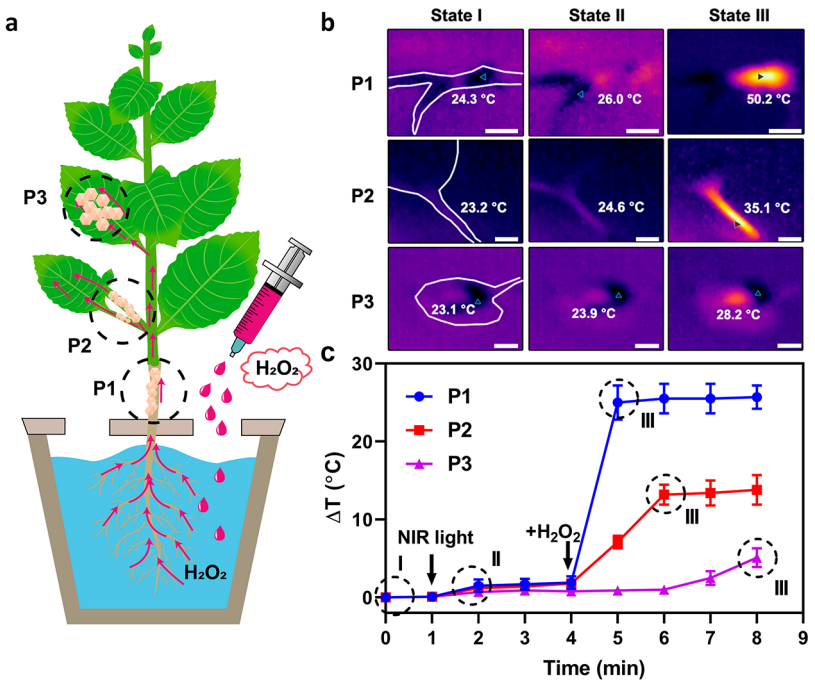

Figure 4. Analysis of H_2O_2 transport *in vivo* using the ZIF-8 biosensor. (a) Schematic illustration of assembled ZIF-8 biosensors in *Nb*'s designated position (P1−P3). With a final concentration of 1 mM H_2O_2 in the hydroponic culture medium, H_2O_2 could diffuse from root cell walls and membranes to the upper organs. (b) Thermal imaging of ZIF-8 biosensors at P1−P3 under NIR light irradiation (808 nm, 2 W cm^{-2}). The white lines outlined *Nb* organs. Scale bar: 1 cm. (c) Thermal response of ZIF-8 biosensors at P1−P3 before and after NIR light irradiation (808 nm, 2 W cm^{-2}). At the fourth minute, 1 mM H_2O_2 was added to the hydroponic culture medium.

plants.[61] Plant hormones, such as indoleacetic acid (IAA), salicylic acid (SA), and abscisic acid (AA), are growth regulators of plants and can also regulate plant stress on the environment.[62] Interestingly, other than H_2O_2, the ZIF-8 biosensor did not respond to other plant metabolites based on the unchanged temperature (Figure S16). However, the temperature increased to 51.7 °C after applying our ZIF-8 biosensor in the presence of H_2O_2, demonstrating that our biosensor had good selectivity for H_2O_2 detection due to the presence of HRP within the ZIF-8 exoskeleton.

Thermal Analysis of Exogenous H_2O_2 Transport in Plant Organs. Considering that H_2O_2, a small polar molecule, can diffuse across cell walls and membranes, transport through the vascular system of plants, and even diffuse away from plant organs to the extracellular space,[48] our ZIF-8 biosensor was used to monitor H_2O_2 transport in plant organs. ZIF-8 biosensors were assembled at three designated positions on an *Nb* from bottom to top: site adjacent to roots not immersed in H_2O_2 solution (P1), petiole (P2), and leaf (P3). After that, H_2O_2 with a final concentration of 1 mM was added to *Nb*'s hydroponic culture medium for subsequent H_2O_2 transport studies (Figure 4a).

Parts b and c of Figure 4 showed that ZIF-8 biosensors kept silent for P1−P3 at zero time point (State I, no H_2O_2, and no NIR light irradiation). Then, NIR light irradiation was applied, and negligible temperature increases were at 2 min time point (State II, no H_2O_2, but with NIR light irradiation). In contrast, after adding H_2O_2 into the hydroponic culture medium (State III, with H_2O_2 and NIR light irradiation), the thermal signal of ZIF-8 biosensors at P1 (about 1 cm away from roots) immediately increased. The naked eyes could see even the color change of the ZIF-8 biosensor, indicating that a large amount of H_2O_2 diffused from *Nb*'s roots to its stem. Similarly, the ZIF-8 biosensor at P2 was fully activated within 2 min. The thermal signal at P2 was lower than that at P1. We hypothesized that the concentration of H_2O_2 in petiole would decrease over long-distance transport in the plant vascular system. For the ZIF-8 biosensor at P3, there was a moderate leaf thermal signal change (corresponding to 2.6 μM H_2O_2) after 4 min of incubation. Overall, several significant conclusions are obtained: (1) H_2O_2 can absorb on roots, transport through the vascular system, and diffuse away from *Nb*'s organs to the extracellular space, along with the ZIF-8 biosensor activation; (2) this delayed thermal signal response reflects long-distance transport of H_2O_2 from roots to leaves, which can be completed within several minutes; (3) most of H_2O_2 in leaves are probably decomposed through the enzyme-mediated decomposition reaction because the concentration of H_2O_2 measured in leaves is significantly less than that in stem and petiole.[63] Considering 1 mM H_2O_2 might be a high concentration to test, we also studied less exogenous H_2O_2 (150 μM) transport in plant organs. As shown in Figure S17, ZIF-8 biosensors at P1−P3 still could report the temperature changes. Among the three sites, the temperature change at the root was the most obvious (ΔT = 6.2 °C). In addition to detecting H_2O_2 through color-to-thermal signal conversion, two other approaches were used to validate our method, either using a general H_2O_2 assay kit or 3,3′-diaminobenzidine (DAB) to stain *Nb* leaves, demonstrating consistency with the trend of our biosensor (Figure S18). In the H_2O_2 kit, H_2O_2 could react with titanium sulfate, and products were measured at a colorimetric readout at 415 nm. For the DAB staining method, H_2O_2 can oxidize DAB with some haem-containing proteins to generate a dark brown precipitate. Therefore, our ZIF-8 biosensor can effectively detect exogenous H_2O_2

https://doi.org/10.1021/acsnano.2c06481
ACS Nano 2022, 16, 15175−15187

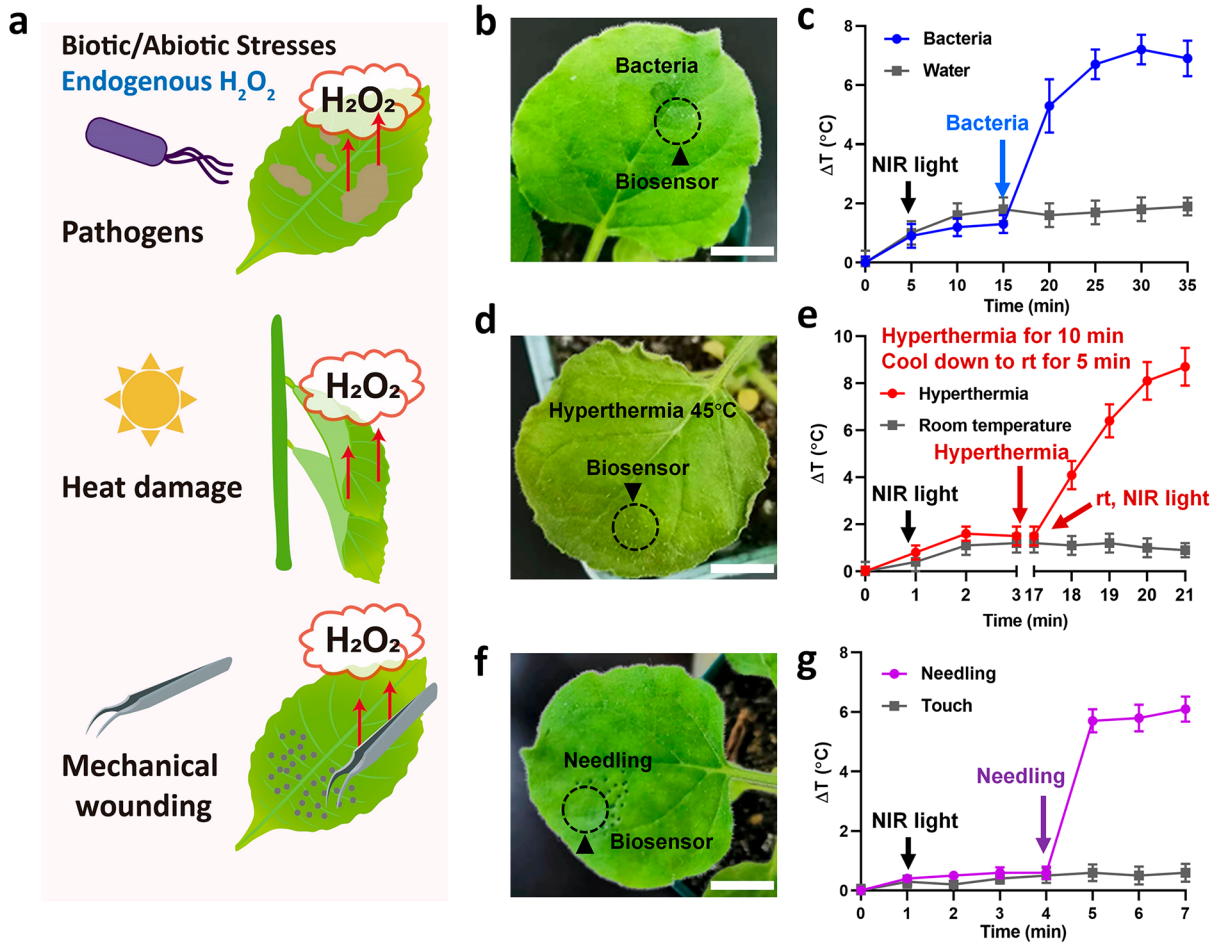

Figure 5. Thermal analysis of plant health with endogenous H_2O_2 produced under biotic and abiotic stresses using ZIF-8 biosensors. (a) Schematic illustration of biotic and abiotic stresses producing endogenous H_2O_2 in leaves. The thermal response of the ZIF-8 biosensor in leaves indicating the onset of biotic or abiotic stresses, such as (b and c) *P. syringae*, (d and e) high temperature (45 °C), and (f and g) mechanical wounding. Scale bar: 1 cm.

transport in plant organs through color-to-thermal signal conversion.

Thermal Analysis of Endogenous H_2O_2 Caused by Plant Biotic or Abiotic Stresses. Having confirmed the feasibility of the ZIF-8 biosensor for detecting H_2O_2, we used the ZIF-8 biosensor to monitor plant health with endogenous H_2O_2 produced under biotic and abiotic stresses, including *Pseudomonas syringae* (*P. syringae*), high temperature (45 °C), and mechanical wounding (Figure 5a). The phytopathogenic bacterium *P. syringae* causes severe diseases in many important crop plants, secreting disease-causing factors with biotic stress.[64] Heat stress and mechanical wounding can induce H_2O_2 accumulating in the intracellular region, inducing severe cellular damage and affecting plant growth and development.[13,65]

The negative control was touching or spraying hydroponic culture medium onto *Nb*'s leaves. No apparent changes were observed compared to the environment background signal, indicating the low level of H_2O_2 in healthy organs. Before applying biotic or abiotic stresses on *Nb* leaves, the temperature of *Nb* leaves showed insignificant increases under NIR light irradiation (ΔT = 0.6 °C), suggesting that NIR light irradiation alone did not induce any endogenous H_2O_2 production (Figure 5c,e,g). Mechanical injection of *P. syringae* into the *Nb* mesophyll showed a significant thermal signal increase, which could reach a plateau within 20 min (ΔT = 7.2 °C) (Figure 5b,c). High-temperature stress can induce the production of H_2O_2 and causes severe damage to plants. We put *Nb* in a high-temperature culture chamber for 10 min at 45 °C. Next, *Nb* was taken out until it came back to room temperature. The thermal signal of the ZIF-8 biosensor was recorded. The temperature of the ZIF-8 biosensor site rapidly increased within 4 min (ΔT = 8.7 °C, corresponding to 5.9 μM H_2O_2) (Figure 5d,e). For the mechanical wounding, the temperature of the ZIF-8 biosensor site increased by 6.1 °C within 1 min under NIR light irradiation (ΔT = 6.1 °C, corresponding to 3.9 μM H_2O_2) (Figure 5f,g). Interestingly, H_2O_2 production by bacteria was slower than that by heat damage or mechanical wounding, and the production of H_2O_2 under high temperatures was associated with other leaves (Figure S19a). In contrast, mechanical wounding and pathogenic microorganism infection were merely associated with a single leaf having a locally increased concentration of H_2O_2 (Figure S19b,c). We also applied stress treatment and NIR light to *Nb* leaves without ZIF-8 biosensors or with pure ZIF-8 (negative controls). The temperature increase was quite limited, and *Nb* leaf temperature could increase due to the stresses themselves (Figure S20). Therefore, H_2O_2 production time and thermal signals reflected distinct H_2O_2 production pathways under biotic and abiotic stresses. It was worth noting

https://doi.org/10.1021/acsnano.2c06481
ACS Nano 2022, 16, 15175−15187

that endogenous H_2O_2 under biotic and abiotic stresses diffused from inner organs, which might be why H_2O_2 induced by stresses was lower than previously reported concentrations.[13,24] Even so, our ZIF-8 biosensor was sensitive enough to monitor H_2O_2 production caused by various stresses, which could be used to monitor plant health. In addition, three widely cultivated plant species, *i.e.*, tomato, kiwi, and strawberry, were used to evaluate the plant health with endogenous H_2O_2 produced under mechanical wounding using our biosensors. The temperature of the ZIF-8 biosensor site increased by 4.3 °C within 2 min for tomato and 3.0 and 3.1 °C within 1 min for kiwi and strawberry under NIR light irradiation, demonstrating our biosensor's universality (Figure S21).

CONCLUSION

In summary, we developed a ZIF-8 biosensor for simple, convenient, and *in situ* detection of H_2O_2 in plants. We demonstrated that the ZIF-8 biosensor containing HRP and ABTS could be assembled on a plant root, petiole, or leaf using a simple spray method. This biosensor could report submicromolar H_2O_2 in plants through color-to-thermal signal conversion. Temperature changes through oxidizing ABTS with the help of HRP and H_2O_2 were treated as the signal readout under the NIR light irradiation, which eliminated plant high background color and autofluorescence interference, significantly improving the S/N ratio. These ZIF-8 biosensors are applied in not only remote thermal sensing of exogenous H_2O_2 transport in plant organs but also endogenous H_2O_2 caused by plant biotic or abiotic stresses. Other than H_2O_2, other signal molecules, such as nitric oxide, molecular oxygen, adenosine triphosphate, strigolactones, dopamine, phytoestrogens, and so on, play a cruical role in plant health, including growth and development, metabolism, cell death, and stress response.[19] Our biosensor can be used for the future development of plant sensors for monitoring plant signaling pathways and metabolism that are nondestructive, minimally invasive, and capable of real-time, *in situ* analysis. It can be translated to crop plant species for agriculture applications.[66,67] However, there will be many challenges for plant biosensors in field conditions.[68] Large-scale field demonstrations under agricultural conditions are critically needed to understand biosensors' feasibility and limitations. Future work is required for plant biosensors in field conditions over the long-term. With the development of the Internet of Things, fifth-generation communication, artificial intelligence, and machine learning, real-time, dynamic, and intelligent detection of plant signals pathways and metabolism can be deeply integrated with these technologies to build an intelligent agricultural big data management platform for long-term monitoring of crop physiological changes, air contaminant monitoring, and realizing the optimal management of crop growth.[69,70]

METHODS

Materials. $ZnAc_2$, H_2O_2, 2-methylimidazole (2-mim), horseradish peroxidase (HRP), 2,2′-azino-bis(3-ethylbenzothiazoline-6-sulfonic acid) (ABTS), glucose (Glu), $CaCl_2$, indoleacetic acid (IAA), salicylic acid (SA), and abscisic acid (AA) were obtained from Aladdin Reagent (Shanghai, China). Bicinchoninic acid (BCA) protein assay kit was purchased from Beyotime Biotechnology (Shanghai, China). Milli-Q (18.2 MΩ) water was used to prepare the buffers and solutions. All other reagents and solvents were of analytical grade and used as received.

Plant Growth. *Nb* seeds, obtained from Prof. Zhang Zhaoliang's Lab, Anhui Agricultural University, were germinated and grown in a carbon dioxide artificial climate chamber (CRD-C2000, Darthcarter, China). The plants were grown in 4 in. pots under LED light and a 16/8 light/dark photoperiod at 23 °C and 60% humidity. Before experimental use, plants were allowed to mature to 3−4 weeks of age within the chamber. Tomato (*Solanum lycopersicum* L.) cv. Ailsa Craig and kiwi (*Actinidia chinensis*) cv. Hongyang were obtained from Prof. Miao Min's Lab, Hefei University of Technology. Strawberry (*Fragaria vesca* L.) cv. yellow wonder was obtained from Prof. Zhang Hua's Lab, Hefei University of Technology. These plants were germinated and grown in the glasshouse under artificial conditions under LED light and a 16/8 light/dark photoperiod with a temperature >22 °C and 60% humidity.

Bacterial Culture. A single *Pseudomonas syringae* (*P. syringae*) strain colony was inoculated and grown in 5 mL of Luria−Bertani (LB) media overnight under aerobic conditions. After overnight incubation, the bacterial solution was centrifuged and washed twice with sterile water. Finally, the bacteria were resuspended in a 20% LB liquid medium and stored in a refrigerator at 4 °C.

ZIF-8 Assembly on Plant Organs. Plant organs were first washed with Milli-Q water to remove impurities. Our biosensor was constructed with four components (ABTS, HRP, 2-mim, and $ZnAc_2$) in two household sprayers and assembled on plant organs *via* a spray method. Within the first sprayer, we mixed ABTS, HRP, and 2-mim, incubating them for 10 min. The final concentrations of ABTS, HRP, and 2-mim were 2 mg mL^{-1}, 15 μg mL^{-1}, and 70 mM, respectively. This mixture was sprayed on the plant leaf, petiole, or root using a household sprayer for 3 s. After waiting for 3 min, 40 mM $ZnAc_2$ solution was sprayed on the same site for 2 s and rested for 5 min, generating the ZIF-8 biosensor. Finally, excess ZIF-8 was thoroughly washed away by repeated washing at least three times. HRP/ABTS, $ZnAc_2$/2-mim, $ZnAc_2$/2-mim/HRP, and untreated *Nb* organs were used as control groups. *Nb* organs were then imaged using Sony Alpha NEX-5N digital camera.

Encapsulation Efficiencies of HRP and ABTS. ABTS (2 mg mL^{-1}), HRP (15 μg mL^{-1}), $ZnAc_2$ (20 mM), and 2-mim (1.7 mg mL^{-1}) were mixed to generate the ZIF-8 biosensor. After 5 min of incubation, the supernatant solution was collected by centrifugation, and the absorption values were recorded by an ultraviolet−visible (UV−vis) spectrophotometer (PerkinElmer) or a fluorescence microplate reader (Infinite M200, Tecan). For ABTS, the encapsulation efficiency was calculated by the ratio of OD_{808} and the ABTS (2 mg mL^{-1}) solution as a control. For HRP, the encapsulation efficiency was calculated by BCA kit according to the manufacturer's instruction.

Scanning Electron Microscope. The obtained *Nb* organ ZIF-8 biosensors were fixed with 5% paraformaldehyde solution overnight. The *Nb* leaf, petiole, or root was then dehydrated with ethanol using a series of concentrations (30, 50, 70, 80, 95, and 100% for 20 min, respectively). Finally, plant organs with a thin coat of Au/Pd in a sputter coater were examined under a field emission SEM (Hitachi SU8020), and the elements of C, N, and Zn were measured with energy-dispersive X-ray analysis. SEM image and EDS results of ZIF-8 in an aqueous solution were also obtained.

Microscopy Z-Stack Image. To prove that HRP was embedded in the ZIF-8 exoskeleton, rhodamine-labeled HRP (Rh-HRP) was instead used for fluorescence imaging. A Rh-labeled ZIF-8 biosensor was obtained after centrifugation at 14,000 rpm to remove free Rh-HRP for 10 min. Furthermore, a layer-by-layer scanning manner along the *z*-axis position by CLSM was performed to construct the three-dimensional distribution of Rh-HRP inside the ZIF-8 exoskeleton.

X-ray Diffraction (XRD) Experiments. To demonstrate whether HRP and ABTS encapsulation affects the crystal structure of ZIF-8, 100 mg of pure ZIF-8 or ZIF-8 biosensor powder was used, and XRD measurements were carried out using a Bruker AXS D8 advance powder diffractometer with Cu-Kα X-ray radiation from 10° to 90°.

Stability of HRP and ZIF-8 Biosensor Coated on *Nb* Roots. To explore whether the ZIF-8 exoskeleton could remain the catalytic activity of HRP, we conducted several harsh treatments on ZIF-8-

https://doi.org/10.1021/acsnano.2c06481
ACS Nano 2022, 16, 15175−15187

biosensor-coated *Nb* roots, for example, multirinsing steps, heating at 60 °C for 15 min, long-term storage for 7 days, and trypsin digestion. Next, the treated roots were soaked in 100 μM H_2O_2 solution. The colorimetric signal of the catalytic reaction was monitored using a fluorescence microplate reader, and the absorbance spectra of reacted H_2O_2 solution were recorded on a Lambda 465 UV−vis spectrometer (PerkinElmer). Free HRP was used as the positive control *via* spraying on the *Nb* root. Following the same washing procedure, the root was immersed in the ABTS/H_2O_2 solution (ABTS 2 mg mL^{-1}, H_2O_2 100 μM). HRP (15 μg mL^{-1}) immersed in the ABTS/H_2O_2 (ABTS 2 mg mL^{-1}, H_2O_2 100 μM) solution was also used as a reference for the experiment, having 100% HRP activity.

Safety Evaluation of ZIF-8 Biosensors on *Nb* Leaves. Nb leaves were dark-adapted for 30 min for chlorophyll fluorescence analysis. The *Nb* leaf was treated with the ZIF-8 biosensor or its components for the designated time (0, 2, 5, and 10 min). The component concentrations were 15 μg mL^{-1} and 2 mg mL^{-1} for HRP and ABTS. Pure ZIF and 1 mM H_2O_2 were used as the negative and positive controls, respectively. Chlorophyll fluorescence yield (F_V/F_M) was measured using an imaging pulse amplitude modulated fluorimeter (IMAG-MAXI; Heinz Walz, Effeltrich, Germany). Transient chlorophyll fluorescence induction curves were obtained using a Yaxin-1161G fluorometer (Yaxin, YaXin Liyi Technology Co., Beijing, China).

Quantitative polymerase chain reaction (qPCR) was also used to investigate the biocompatibility of the ZIF-8 biosensor. Total RNA was extracted from the plant leaf using the RNAprep Pure Kit DP432 (TianGen, Beijing, China), following the manufacturer's instructions. Next, RNA was reverse-transcribed to cDNA, and qPCR analysis was performed with 2x Fast qPCR Master Mix (High Rox, B639273, BBI) using a fluorescent quantitative PCR instrument (ABI). The gene expression levels were measured and analyzed by the 2-ΔΔCt method.

The stress indicator gene NbrbohB primers used were:

- forward 5′-TTTCTCTGAGGTTTGCCAGCCACCACC-TAA-3′
- reverse 5′-GCCTTCATGTTGTTGACAATGTCTTTAACA-3′

Primers for the housekeeping gene elongation factor 1 (EF1) were:

- forward 5′-TGGTGTCCTCAAGCCTGGTATGGTTGT-3′
- reverse 5′-ACGCTTGAGATCCTTAAC CGCAA-CATTCTT-3′

Detection of H_2O_2 *in Vitro*. To obtain the optimal conditions, the parameters of the ZIF-8 biosensor are optimized. The concentration of ZIF-8 was fixed with final concentrations of 20 mM $ZnAc_2$ and 70 mM 2-mim, and that of H_2O_2 was 100 μM. To determine the optimal concentration of ABTS (0−2 mg mL^{-1}), other parameters were 15 μg mL^{-1} HRP, reaction time 5 min, and NIR irradiation (808 nm, 2 W cm^{-2}). To determine the optimal concentration of HRP (0−45 μg mL^{-1}), other parameters were 2 mg mL^{-1} ABTS, reaction time 5 min, and NIR irradiation (808 nm, 2 W cm^{-2}). To determine the optimal ZIF-8 formation time (5−60 min), other parameters were 15 μg mL^{-1} HRP, 2 mg mL^{-1} ABTS, and NIR irradiation (808 nm, 2 W cm^{-2}). To determine the optimal NIR laser power (0−3 W cm^{-2}), other parameters were 15 μg mL^{-1} HRP, 2 mg mL^{-1} ABTS, and reaction time 5 min. To detect H_2O_2 *in vitro*, different concentrations of H_2O_2 (0−100 μM) were added to the ZIF-8 biosensor with the optimal condition, *i.e.*, 15 μg mL^{-1} HRP, 2 mg mL^{-1} ABTS, reaction time 5 min, and NIR irradiation (808 nm, 2 W cm^{-2}). UV−vis spectrophotometer and thermal images were used to obtain the above-mentioned data. To detect the limit of detection (LOD) for pure HRP, a 100 μL mixture of 15 μg mL^{-1} HRP and 2 mg mL^{-1} ABTS was prepared, and different concentrations of H_2O_2 were added (final concentration: 0, 1.25, 2.5, 5, 10, and 25 μM). After 5 min incubation, the absorbance values were recorded by a UV−vis spectrometer. The LOD was calculated according to blank signal plus 3 × standard deviations. The above experiments were repeated three times.

Specificity of the ZIF-8 Biosensor. To demonstrate the specificity of the ZIF-8 biosensor, Glu, Suc, Ca^{2+}, IAA, SA, AA, or H_2O_2 with a final concentration of 100 μM was added to the ZIF-8 biosensor solution. Then, each solution was irradiated under NIR light irradiation (808 nm, 2 W cm^{-2}) for up to 40 s. The NIR irradiation source was purchased from Changchun Institute of Optics (FU808ADX-F34, Changchun, China). Thermal images and signals were collected using a hand-held infrared thermometer (H10, Hikvision).

Thermal Analysis of Exogenous H_2O_2 on Different Plant Organs. To *in situ* detect exogenous H_2O_2 on plant organs, the ZIF-8 biosensor assembled *Nb* leaf, petiole, or root was under NIR light irradiation (808 nm, 2 W cm^{-2}) for up to 40 s with or without adding a drop of H_2O_2 (5 μL, 50 μM) solution. To obtain the calibration curves of leaf, petiole, and root sensors for H_2O_2 detection, up to 100 μM of H_2O_2 were mixed with ZIF-8 biosensors. Thermal signal changes were recorded using an infrared thermometer under NIR light irradiation (808 nm, 2 W cm^{-2}). The stability of the ZIF-8 biosensor on *Nb* leaves under long-term storage for up to 8 days with exogenous H_2O_2 (5 μL, 100 μM) was also detected through color-to-thermal signal conversion. To investigate the relationship between ZIF-8 biosensor thickness and its sensing performance, the reactants were sprayed onto *Nb* leaves for 3 s each time. After spraying up to five times, excess ZIF-8 was washed away. Thermal analysis experiments were conducted by adding a drop of H_2O_2 (5 μL, 10−50 μM) solution. The subsequent procedures were the same as the experiments mentioned above.

H_2O_2 Transport Study. ZIF-8 biosensors were assembled at three designated positions on an *Nb*. The biosensor on the stem, 1 cm away from the roots, was recognized as Position 1 (P1) sensor. Biosensor on the petiole, 6 cm away from P1, was recognized as Position 2 (P2) sensor. Biosensor on the leaf, 1.5 cm away from P2, was recognized as Position 3 (P3). Before the thermal analysis, the *Nb* was transferred to a 200 mL container with pure water for 10 min. The background thermal signals at three positions were measured. At the fourth minute, 20 or 3.3 μL of 10 M H_2O_2 solution was injected into the container. Thermal signal changes in three positions were recorded using an infrared thermometer under NIR light irradiation (808 nm, 2 W cm^{-2}). To further validate the transport of H_2O_2, *Nb* leaves (100−200 mg) were cut at 4 and 8 min after adding H_2O_2 in the container with a final concentration of 1 mM. Next, *Nb* leaves were ground with 1 mL of acetone in liquid nitrogen. The concentration (μmol/g fresh weight) of extracted H_2O_2 was determined using a general H_2O_2 assay kit (Sangon Biotech, Shanghai, China). In this kit, H_2O_2 reacted with titanium sulfate, and products could be measured at a colorimetric readout at 415 nm. One micromolar H_2O_2 was used as a standard reference. Another approach is to use 3,3′-diaminobenzidine (DAB) to stain *Nb* leaves. H_2O_2 can oxidize DAB with some haem-containing proteins to generate a dark brown precipitate. *Nb* leaves cut at 4 or 8 min were soaked in 1 mg mL^{-1} DAB solution and gently vacuumed for the DAB infiltration. After 3 h of incubation, *Nb* leaves were decolorized with 100% ethanol overnight and then photographed using a digital camera.

Monitoring Plant Stress-Induced H_2O_2. Four *Nb* leaves are used for each set of experiments. For the biotic stress model, *Nb* leaves were inoculated with *P. syringae* (200 μL, 10^9 CFU mL^{-1}), and the plants were incubated under the standard *Nb* growth conditions described above. For the abiotic stress model, we put the *Nb* in a high-temperature culture chamber for 10 min at 45 °C. Next, the *Nb* was taken out until it returned to room temperature. Mechanical wounding was induced using forceps to poke many holes in the leaf lamina. Then, thermal signal changes of ZIF-8 biosensors were recorded using an infrared thermometer under NIR light irradiation (808 nm, 2 W cm^{-2}). In addition, we selected four leaves on the same *Nb*: L1, the stressed leaf; L2, the leaf parallel to L1 laterally; L3, the leaf on top of L1; L4, the leaf below L1. The level of H_2O_2 in *Nb* leaves (L1−L4) was monitored with the method mentioned above. In addition, tomato, strawberry, and kiwi leaves were used to evaluate the plant health with endogenous H_2O_2 produced under mechanical

https://doi.org/10.1021/acsnano.2c06481
ACS Nano 2022, 16, 15175−15187

wounding using our biosensors. All procedures were same as that of *Nb* leaves.

ASSOCIATED CONTENT

Supporting Information

The Supporting Information is available free of charge at https://pubs.acs.org/doi/10.1021/acsnano.2c06481.

Figures of assembly of the ZIF-8 biosensor on *Nb* organs, SEM image and EDS of ZIF-8 in an aqueous solution, 3D reconstructed image of HRP/ZIF-8 using CLSM, optimization of experimental conditions, control experiments, sensing performance depending on the thickness of the ZIF-8 biosensor, specificity of ZIF-8 biosensors, and more H_2O_2 detection and transport study, and thermal analysis of plant health with stress treatments and table of definition of chlorophyll fluorescence parameters (PDF)

AUTHOR INFORMATION

Corresponding Authors

Chao Li − *School of Food and Biological Engineering, Hefei University of Technology, Hefei, Anhui 230009, P. R. China;* orcid.org/0000-0002-2552-413X; Email: lchao@hfut.edu.cn

Feng Wang − *School of Food and Biological Engineering, Hefei University of Technology, Hefei, Anhui 230009, P. R. China;* orcid.org/0000-0002-2796-5473; Email: fengw420@hfut.edu.cn

Authors

Yong Yan − *School of Food and Biological Engineering, Hefei University of Technology, Hefei, Anhui 230009, P. R. China*

Min Ni − *School of Food and Biological Engineering, Hefei University of Technology, Hefei, Anhui 230009, P. R. China*

Fan Wang − *School of Food and Biological Engineering, Hefei University of Technology, Hefei, Anhui 230009, P. R. China*

Yue Yu − *School of Food and Biological Engineering, Hefei University of Technology, Hefei, Anhui 230009, P. R. China*

Xin Gong − *School of Food and Biological Engineering, Hefei University of Technology, Hefei, Anhui 230009, P. R. China*

Yue Huang − *College of Light Industry and Food Engineering, Nanjing Forestry University, Nanjing 210037, P. R. China*

Wei Tao − *School of Food and Biological Engineering, Hefei University of Technology, Hefei, Anhui 230009, P. R. China*

Complete contact information is available at: https://pubs.acs.org/10.1021/acsnano.2c06481

Author Contributions

[§]Y.Yan, M.Ni, and F.Wang contributed equally. The manuscript was written through the contributions of all authors.

Notes

The authors declare no competing financial interest.

ACKNOWLEDGMENTS

This work was supported by the National Natural Science Foundation of China (31971314), the Fundamental Research Funds for the Central Universities of China (JZ2021HGTB0120), the Distinguished Youth Foundation of Anhui Province (1808085J05), and the Key Research and Development Plan of Anhui Province (202104b11020015).

REFERENCES

(1) Piao, S. L.; Ciais, P.; Huang, Y.; Shen, Z. H.; Peng, S. S.; Li, J. S.; Zhou, L. P.; Liu, H. Y.; Ma, Y. C.; Ding, Y. H.; Friedlingstein, P.; Liu, C. Z.; Tan, K.; Yu, Y. Q.; Zhang, T. Y.; Fang, J. Y. The Impacts of Climate Change on Water Resources and Agriculture in China. *Nature* **2010**, *467*, 43−51.

(2) Chakraborty, S.; Newton, A. C. Climate Change, Plant Diseases and Food Security: An Overview. *Plant Pathol.* **2011**, *60*, 2−14.

(3) Zandalinas, S. I.; Fritschi, F. B.; Mittler, R. Climate Change, and Environmental Pollution: Recipe for a Multifactorial Stress Combination Disaster. *Trends Plant Sci.* **2021**, *26*, 588−599.

(4) Peñuelas, J.; Filella, I. Visible and Near-Infrared Reflectance Techniques for Diagnosing Plant Physiological Status. *Trends Plant Sci.* **1998**, *3*, 151−156.

(5) Jetz, W.; Cavender-Bares, J.; Pavlick, R.; Schimel, D.; Davis, F. W.; Asner, G. P.; Guralnick, R.; Kattge, J.; Latimer, A. M.; Moorcroft, P.; Schaepman, M. E.; Schildhauer, M. P.; Schneider, F. D.; Schrodt, F.; Stahl, U.; Ustin, S. L. Monitoring Plant Functional Diversity from Space. *Nature Plants* **2016**, *2*, 16024.

(6) Roper, J. M.; Garcia, J. F.; Tsutsui, H. Engineering the Drug Carrier Biointerface to Overcome Biological Barriers to Drug Delivery. *ACS Omega* **2021**, *6*, 5101−5107.

(7) Ali, M. A.; Dong, L.; Dhau, J.; Khosla, A.; Kaushik, A. Perspective—Electrochemical Sensors for Soil Quality Assessment. *J. Electrochem. Soc.* **2020**, *167*, 037550.

(8) Nehra, M.; Dilbaghi, N.; Marrazza, G.; Kaushik, A.; Sonne, C.; Kim, K. H.; Kumar, S. Emerging Nanobiotechnology in Agriculture for the Management of Pesticide Residues. *J. Hazard. Mater.* **2021**, *401*, 123369.

(9) Mittler, R.; Vanderauwera, S.; Suzuki, N.; Miller, G.; Tognetti, V. B.; Vandepoele, K.; Gollery, M.; Shulaev, V.; Breusegem, F. V. ROS Signaling: The New Wave? *Trends Plant Sci.* **2011**, *16*, 300−309.

(10) Choudhury, F. K.; Rivero, R. M.; Blumwald, E.; Mittler, R. Reactive Oxygen Species, Abiotic Stress and Stress Combination. *Plant J.* **2017**, *90*, 856−867.

(11) Miller, G.; Schlauch, K.; Tam, R.; Cortes, D.; Torres, M. A.; Shulaev, V.; Dangl, J. L.; Mittler, R. The Plant NADPH Oxidase RBOHD Mediates Rapid Systemic Signaling in Response to Diverse Stimuli. *Sci. Signal.* **2009**, *2*, ra45.

(12) Niemeyer, J.; Scheuring, D.; Oestreicher, J.; Morgan, B.; Schroda, M. Real-Time Monitoring of Subcellular H_2O_2 Distribution in *Chlamydomonas reinhardtii*. *Plant Cell* **2021**, *33*, 2935−2949.

(13) Lew, T. T. S.; Koman, V. B.; Silmore, K. S.; Seo, J. S.; Gordiichuk, P.; Kwak, S.-Y.; Park, M.; Ang, M. C.-Y.; Khong, D. T.; Lee, M. A.; Chan-Park, M. B.; Chua, N.-H.; Strano, M. S. Real-Time Detection of Wound-Induced H_2O_2 Signalling Waves in Plants with Optical Nanosensors. *Nat. Plants* **2020**, *6*, 404−415.

(14) Zulfugarov, I. S.; Tovuu, A.; Kim, J. H.; Lee, C. H. Detection of Reactive Oxygen Species in Higher Plants. *J. Plant Biol.* **2011**, *54*, 351−357.

(15) Ortega-Villasante, C.; Buren, S.; Baron-Sola, A.; Martinez, F.; Hernandez, L. E. In vivo ROS and Redox Potential Fluorescent Detection in Plants: Present Approaches and Future Perspectives. *Methods* **2016**, *109*, 92−104.

(16) Olson, P. D.; Varner, J. E. Hydrogen Peroxide and Lignification. *Plant J.* **1993**, *4*, 887−892.

(17) Sun, L. J.; Pan, Y.; Wu, J.; Zhao, D. Y.; Hui, M. Q.; Zhu, S. Q.; Zhu, X. Y.; Li, D. Y.; Song, F. M.; Zhang, C. K. Paper-Based Analytical Devices for the Rapid and Direct Electrochemical Detection of Hydrogen Peroxide in Tomato Leaves Inoculated with *Botrytis cinerea*. *Sensors* **2020**, *20*, 5512.

(18) Donaldson, L. Autofluorescence in Plants. *Molecules* **2020**, *25*, 2393.

(19) Kwak, S. Y.; Wong, M. H.; Lew, T. T. S.; Bisker, G.; Lee, M. A.; Kaplan, A.; Dong, J. Y.; Liu, A. T. X.; Koman, V. B.; Sinclair, R.; Hamann, C.; Strano, M. S. Nanosensor Technology Applied to Living Plant Systems. *Annual Rev. Anal. Chem.* **2017**, *10*, 113−140.

(20) Giraldo, J. P.; Wu, H. H.; Newkirk, G. M.; Kruss, S. Nanobiotechnology Approaches for Engineering Smart Plant Sensors. *Nat. Nanotechnol.* **2019**, *14*, 541−553.
(21) Yang, C. W.; Hu, Y.; Yuan, L.; Zhou, H. Z.; Sheng, G. P. Selectively Tracking Nanoparticles in Aquatic Plant Using Core-Shell Nanoparticle-Enhanced Raman Spectroscopy Imaging. *ACS Nano* **2021**, *15*, 19828−19837.
(22) Lee, G.; Wei, Q. S.; Zhu, Y. Emerging Wearable Sensors for Plant Health Monitoring. *Adv. Mater. Funct.* **2021**, *31*, 2106475.
(23) Lew, T. T. S.; Koman, V. B.; Gordiichuk, P.; Park, M.; Strano, M. S. The Emergence of Plant Nanobionics and Living Plants as Technology. *Adv. Mater. Technol.* **2020**, *5*, 1900657.
(24) Wu, H. H.; Nissler, R.; Morris, V.; Herrmann, N.; Hu, P. G.; Jeon, S. J.; Kruss, S.; Giraldo, J. P. Monitoring Plant Health with Near-Infrared Fluorescent H_2O_2 Nanosensors. *Nano Lett.* **2020**, *20*, 2432−2442.
(25) Furukawa, H.; Cordova, K. E.; O'Keeffe, M.; Yaghi, O. M. The Chemistry and Applications of Metal-Organic Frameworks. *Science* **2013**, *341*, 1230444.
(26) Sun, L.; Campbell, M. G.; Dinca, M. Electrically Conductive Porous Metal-Organic Frameworks. *Angew. Chem., Int. Ed.* **2016**, *55*, 3566−3579.
(27) Liang, W. B.; Wied, P.; Carraro, F.; Sumby, C. J.; Nidetzky, B.; Tsung, C. K.; Falcaro, P.; Doonan, C. J. Metal-Organic Framework-Based Enzyme Biocomposites. *Chem. Rev.* **2021**, *121*, 1077−1129.
(28) Li, Y. T.; Zhang, K.; Liu, P. R.; Chen, M.; Zhong, Y. L.; Ye, Q. S.; Wei, M. Q.; Zhao, H. J.; Tang, Z. Y. Encapsulation of Plasmid DNA by Nanoscale Metal-Organic Frameworks for Efficient Gene Transportation and Expression. *Adv. Mater.* **2019**, *31*, 1901570.
(29) Doonan, C.; Ricco, R.; Liang, K.; Bradshaw, D.; Falcaro, P. Metal-Organic Frameworks at the Biointerface: Synthetic Strategies and Applications. *Acc. Chem. Res.* **2017**, *50*, 1423−1432.
(30) Liang, K.; Richardson, J. J.; Cui, J. W.; Caruso, F.; Doonan, C. J.; Falcaro, P. Metal-Organic Framework Coatings as Cytoprotective Exoskeletons for Living Cells. *Adv. Mater.* **2016**, *28*, 7910−7914.
(31) Liang, K.; Ricco, R.; Doherty, C. M.; Styles, M. J.; Bell, S.; Kirby, N.; Mudie, S.; Haylock, D.; Hill, A. J.; Doonan, C. J.; Falcaro, P. Biomimetic Mineralization of Metal-Organic Frameworks as Protective Coatings for Biomacromolecules. *Nat. Commun.* **2015**, *6*, 7240.
(32) Feng, Y. F.; Wang, H. R.; Zhang, S. N.; Zhao, Y.; Gao, J.; Zheng, Y. Y.; Zhao, P.; Zhang, Z. J. M.; Zaworotko, J.; Cheng, P.; Ma, S. Q.; Chen, Y. Antibodies@MOFs: An In Vitro Protective Coating for Preparation and Storage of Biopharmaceuticals. *Adv. Mater.* **2019**, *31*, 1805148.
(33) Chen, W. H.; Vázquez-González, M.; Zoabi, A.; Abu-Reziq, R.; Willner, I. Biocatalytic Cascades Driven by Enzymes Encapsulated in Metal-Organic Framework Nanoparticles. *Nat. Catal.* **2018**, *1*, 689−695.
(34) Horcajada, P.; Chalati, T.; Serre, C.; Gillet, B.; Sebrie, C.; Baati, T.; Eubank, J. F.; Heurtaux, D.; Clayette, P.; Kreuz, C.; Chang, J. S.; Hwang, Y. K.; Marsaud, V.; Bories, P. N.; Cynober, L.; Gil, S.; Férey, G.; Couvreur, P.; Gref, R. Porous Metal-Organic-Framework Nanoscale Carriers as a Potential Platform for Drug Delivery and Imaging. *Nat. Mater.* **2010**, *9*, 172−178.
(35) Wu, M. X.; Yang, Y. W. Metal-Organic Framework (MOF)-Based Drug/Cargo Delivery and Cancer Therapy. *Adv. Mater.* **2017**, *29*, 1606134.
(36) Pan, W.; Cui, B. J.; Wang, K. Y.; Shi, M. W.; Lu, F.; Li, N.; Tang, B. ATP-Triggered Mitochondrial Cascade Reactions for Cancer Therapy with Nanoscale Zeolitic Imidazole Framework-90. *Theranostics* **2021**, *11*, 7869−7878.
(37) Gao, P.; Chen, Y. Y.; Pan, W.; Li, N.; Liu, Z.; Tang, B. Antitumor Agents Based on Metal-Organic Frameworks. *Angew. Chem., Int. Ed.* **2021**, *60*, 16763−16776.
(38) Xu, W. Q.; Jiao, L.; Wu, Y.; Hu, L. Y.; Gu, W. L.; Zhu, C. Z. Metal-Organic Frameworks Enhance Biomimetic Cascade Catalysis for Biosensing. *Adv. Mater.* **2021**, *33*, 2005172.
(39) Gao, P.; Lou, R. X.; Liu, X. H.; Cui, B. J.; Pan, W.; Li, N.; Tang, B. Rational Design of a Dual-Layered Metal-Organic Framework Nanostructure for Enhancing the Cell Imaging of Molecular Beacons. *Anal. Chem.* **2021**, *93*, 5437−5441.
(40) Bobbitt, N. S.; Mendonca, M. L.; Howarth, A. J.; Islamoglu, T.; Hupp, J. T.; Farha, O. K.; Snurr, R. Q. Metal-Organic Frameworks for the Removal of Toxic Industrial Chemicals and Chemical Warfare Agents. *Chem. Soc. Rev.* **2017**, *46*, 3357−3385.
(41) Shekhah, O.; Liu, J.; Fischer, R. A.; Wöll, Ch. MOF Thin Films: Existing and Future Applications. *Chem. Soc. Rev.* **2011**, *40*, 1081−1106.
(42) Richardson, J. J.; Liang, K. Nano-Biohybrids: In Vivo Synthesis of Metal-Organic Frameworks inside Living Plants. *Small* **2018**, *14*, 1702958.
(43) Liang, J. Y.; Zulkifli, M. Y. B.; Choy, S.; Li, Y.; Gao, M.; Kong, B.; Yun, J.; Liang, K. Metal-Organic Framework-Plant Nano-biohybrids as Living Sensors for On-Site Environmental Pollutant Detection. *Environ. Sci. Technol.* **2020**, *54*, 11356−11364.
(44) Li, X. J.; Jiang, C. M.; Yao, Y.; Zhang, Q.; Dai, S. F.; Ying, Y. B.; Ping, J. F. Growth-Controllable Triboelectric Nanogenerator Based on Surface-Attached Metal-Organic Framework Layer on Living Leaf. *Small* **2021**, *17*, 2103430.
(45) Azevedo, A. M.; Martins, V. C.; Prazeres, D. M.; Vojinovic, V.; Cabral, J. M.; Fonseca, L. P. Horseradish Peroxidase: A Valuable Tool in Biotechnology. *Biotechnol. Annu. Rev.* **2003**, *9*, 199−247.
(46) Chen, S.; Yan, Y.; Yu, Y.; Wang, Z. F.; Zhu, X. J.; Sun, L. P.; Li, C.; Wang, F. Ferric Ions as a Catalytic Mediator in Metal-EGCG Network for Bactericidal Effect and Pathogenic Biofilm Eradication at Physiological pH. *Adv. Mater. Interfaces* **2021**, *8*, 2101605.
(47) Nißler, R.; Müller, A. T.; Dohrman, F.; Kurth, L.; Li, H.; Cosio, E. G.; Flavel, B. S.; Giraldo, J. P.; Mithöfer, A.; Kruss, S. Detection and Imaging of the Plant Pathogen Response by Near-Infrared Fluorescent Polyphenol Sensors. *Angew. Chem., Int. Ed.* **2022**, *61*, No. e202108373.
(48) Smirnoff, N.; Arnaud, D. Hydrogen Peroxide Metabolism and Functions in Plants. *New Phytol.* **2019**, *221*, 1197−1214.
(49) Demirer, G. S.; Zhang, H.; Matos, J. L.; Goh, N. S.; Cunningham, F. J.; Sung, Y.; Chang, R.; Aditham, A. J.; Chio, L.; Cho, M. J.; Staskawicz, B.; Landry, M. P. High Aspect Ratio Nanomaterials Enable Delivery of Functional Genetic Material without DNA Integration in Mature Plants. *Nat. Nanotechnol.* **2019**, *14*, 456−464.
(50) Crivello, C.; Sevim, S.; Graniel, O.; Franco, C.; Pané, S.; Puigmartí-Luis, J.; Muñoz-Rojas, D. Advanced Technologies for the Fabrication of MOF Thin Films. *Mater, Horiz.* **2021**, *8*, 168−178.
(51) Gorbe, E.; Calatayud, A. Applications of Chlorophyll Fluorescence Imaging Technique in Horticultural Research: A Review. *Sci. Hortic.* **2012**, *138*, 24.
(52) Rolfe, S. A.; Scholes, J. D. Chlorophyll Fluorescence Imaging of Plant-Pathogen Interactions. *Protoplasma* **2010**, *247*, 163−175.
(53) Zhori, A.; Meco, M.; Brandl, H.; Bachofen, R. In Situ Chlorophyll Fluorescence Kinetics as a Tool to Quantify Effects on Photosynthesis in *Euphorbia cyparissias* by a Parasitic Infection of the Rust Fungus *Uromyces pisi*. *BMC Res. Notes* **2015**, *8*, 698.
(54) Krause, G. H.; Weis, E. Chlorophyll Fluorescence and Photosynthesis: The Basics. *Annu. Rev. Plant Physiol. Plant Mol. Biol.* **1991**, *42*, 313−349.
(55) Zushi, K.; Kajiwara, S.; Matsuzoe, N. Chlorophyll a Fluorescence OJIP Transient as a Tool to Characterize and Evaluate Response to Heat and Chilling Stress in Tomato Leaf and Fruit. *Sci. Hortic.* **2012**, *148*, 39−46.
(56) Kalaji, H. M.; Bosa, K.; Kościelniak, J.; Hossain, Z. Chlorophyll a Fluorescence - A Useful Tool for the Early Detection of Temperature Stress in Spring Barley (*Hordeum vulgare* L.). *OMICS* **2011**, *15*, 925−934.
(57) Zhou, X.; Zeng, Y.; Tang, Y. Y.; Huang, Y. M.; Lv, F. T.; Liu, L. B.; Wang, S. Artificial Regulation of State Transition for Augmenting Plant Photosynthesis using Synthetic Light-Harvesting Polymer Materials. *Sci. Adv.* **2020**, *6*, No. eabc5237.

https://doi.org/10.1021/acsnano.2c06481
ACS Nano 2022, 16, 15175−15187

(58) Chen, Q.; Liang, C.; Sun, X. Q.; Chen, J. W.; Yang, Z. J.; Zhao, H.; Feng, L. Z.; Liu, Z. H_2O_2-Responsive Liposomal Nanoprobe for Photoacoustic Inflammation Imaging and Tumor Theranostics via In Vivo Chromogenic Assay. *Proc. Natl. Acad. Sci. U.S.A.* **2017**, *114*, 5343−5348.
(59) Garagounis, C.; Delkis, N.; Papadopoulou, K. K. Unraveling the Roles of Plant Specialized Metabolites: Using Synthetic Biology to Design Molecular Biosensors. *New Phytol.* **2021**, *231*, 1338−1352.
(60) Hanson, J.; Smeekens, S. Sugar Perception and Signaling—An Update. *Curr. Opin. Plant Biol.* **2009**, *12*, 562−567.
(61) Tuteja, N.; Mahajan, S. Calcium Signaling Network in Plants. *Plant Signal Behav.* **2007**, *2*, 79−85.
(62) Waadt, R.; Seller, C. A.; Hsu, P. K.; Takahashi, Y.; Munemasa, S.; Schroeder, J. I. Plant Hormone Regulation of Abiotic Stress Responses. *Nat. Rev. Mol. Cell Biol.* **2022**.
(63) Silva, K. I.; Sales, C. R. G.; Marchiori, P. E. R.; Silveira, N. M.; Machado, E. C.; Ribeiro, R. V. Short-Term Physiological Changes in Roots and Leaves of Sugarcane Varieties Exposed to H_2O_2 in Root Medium. *J. Plant Physiol.* **2015**, *177*, 93−99.
(64) Xin, X. F.; Kvitko, B.; He, S. Y. *Pseudomonas syringae*: What it Takes to be a Pathogen. *Nat. Rev. Microbiol.* **2018**, *16*, 316−328.
(65) Kotak, S.; Larkindale, J.; Lee, U.; Koskull-Döring, P.; Vierling, E.; Scharf, K. D. Complexity of the Heat Stress Response in Plants. *Curr. Opin. Plant Biol.* **2007**, *10*, 310−316.
(66) Zhang, P.; Guo, Z. L.; Ullah, S.; Melagraki, G.; Afantitis, A.; Lynch, I. Nanotechnology and Artificial Intelligence to Enable Sustainable and Precision Agriculture. *Nat. Plants* **2021**, *7*, 864−876.
(67) Yan, Y.; Zhu, X. J.; Yu, Y.; Li, C.; Zhang, Z. L.; Wang, F. Nanotechnology Strategies for Plant Genetic Engineering. *Adv. Mater.* **2022**, *34*, 2106945.
(68) Buriak, J. M.; Liz-Marzán, L. M.; Parak, W. J.; Chen, X. D. Nano and Plants. *ACS Nano* **2022**, *16*, 1681−1684.
(69) Chaudhary, V.; Kaushik, A.; Furukawa, H.; Khosla, A. Review—Towards 5th Generation AI and IoT Driven Sustainable Intelligent Sensors Based on 2D MXenes and Borophene. *ECS Sens. Plus* **2022**, *1*, 013601.
(70) Chaudhary, V.; Ashraf, N.; Khalid, M.; Walvekar, R.; Yang, Y.; Kaushik, A.; Mishra, Y. K. Emergence of Mxene-Polymer Hybrid Nanocomposites as High-Performance Next-Generation Chemiresistors for Efficient Air Quality Monitoring. *Adv. Funct. Mater.* **2022**, *32*, 2112913.

https://doi.org/10.1021/acsnano.2c06481
ACS Nano 2022, 16, 15175−15187